Optical Materials 84 (2018) 504–513

Contents lists available at ScienceDirect

Optical Materials

journal homepage: www.elsevier.com/locate/optmat

Multifunctional possible application of the Er^{3+}/Yb^{3+}-coped Al_2O_3 prepared by recyclable precursor (aluminum can) and also by sol-gel process

Daiane H.S. Reis[a], Edson Pecoraro[b], Fábia Castro Cassanjes[c], Gael Yves Poirier[c], Rogéria Rocha Gonçalves[d], Jennifer Esbenshade[e], Sidney José L. Ribeiro[b], Marco Antônio Schiavon[a], Jefferson Luis Ferrari[a,f,*]

[a] Grupo de Pesquisa em Química de Materiais – (GPQM), Departamento de Ciências Naturais, Universidade Federal de São João del-Rei, Campus Dom Bosco, Praça Dom Helvécio, 74, CEP: 36301-160, São João del-Rei, MG, Brazil
[b] Instituto de Química, UNESP, P.O. Box 355, CEP: 14800-970, Araraquara, SP, Brazil
[c] Research Group of Materials Chemistry, Universidade Federal de Alfenas, Campus de Poços de Caldas, Poços de Caldas, MG, Brazil
[d] Departamento de Química, Faculdade de Filosofia Ciências e Letras de Ribeirão Preto, USP, Avenida Bandeirantes, 3900, 14040-901, Ribeirão Preto, SP, Brazil
[e] Department of Chemistry and Physics, University of Tennessee at Martin, Martin, TN, USA
[f] Desenvolvimento de Materiais Inorgânicos com Terras Raras - DeMITeR, Instituto de Química – (IQ), Universidade Federal de Uberlândia – (UFU), Av. João Naves de Ávila, 2121 – Bairro Santa Mônica, CEP: 38400-902, Uberlândia, MG, Brazil

ARTICLE INFO

Keywords:
Aluminum oxide
Rare earths
Photoluminescence
C-Telecom
Up-conversion

ABSTRACT

The evolution of research on luminescent phosphors led to research on materials doped with rare earth ions (RE^{3+}), not only because of their photoluminescent properties, but also for their potential applications in photonics. The search for new photoluminescent materials has led to an investigation of the photoluminescence of RE^{3+} present in an aluminum oxide (Al_2O_3) matrix. This oxide has a transparent window on the short ultraviolet to near infrared, excellent mechanical properties and good chemical stability. Within this context, this work aims to obtain Al_2O_3: Er^{3+}/Yb^{3+}. The preparation of Al_2O_3: Er^{3+}/Yb^{3+} involved two synthesis processes. For the co-precipitation process, rings of aluminum cans were used as precursors, and for the sol-gel process, the precursor used was tri-sec-butoxide aluminum. From the XRD results, high heat-treatment temperatures were observed to favor the formation of the α-Al_2O_3 phase and low temperatures were observed to favor the formation the γ-Al_2O_3 phase. The analysis of the photoluminescence emission spectra when excited at 980 nm, showed the up-conversion phenomenon with an emission in the visible region. The emission spectra also showed emission between 1400 and 1650 nm, with a maximum at about 1530 nm. The materials exhibit efficient energy absorption in the infrared region, with light emission in the visible region. Furthermore, the spectra show an intense emission in the infrared region assigned to the $^4I_{13/2} \rightarrow {}^4I_{15/2}$ transition of Er^{3+}, demonstrating excellent potential to be used in optical amplifier device at the third telecommunications window.

1. Introduction

During the last few years, luminescent materials have been considered technologically important components, serving as the basics for the functionality and success of many communication, lighting and imaging systems [1–4].

The continuous evolution of research of these materials in nanoscale structures and well controlled devices, has led to research in rare earth (RE^{3+}) doped materials [5–7]. Thus, the luminescence of the RE^{3+} has attracted much attention because of their potential applications in photonics due to their photoluminescent properties, known since the 20th century [8–11]. Such applications include generator imaging devices, traditional lighting devices such as cathode ray tubes, fluorescent lamps, light emitting diodes, field emission displays, lasers [9], solar cells [12], biological markers [6] in sensors technology [13], in uniform fiber Bragg grating (FBG) [14], optical bistable device (OBD) [15], and more.

The RE^{3+} doped host matrix that have photoluminescence properties, have narrow emission lines that come from intraconfigurational f-f transitions due to the weak interaction of electrons with the 4f ligands [16–18]. Transitions involve the partially occupied 4f orbital having transitions forbidden by Laporte rule [19]. However these f-f emissions

* Corresponding author. Desenvolvimento de Materiais Inorgânicos com Terras Raras (DeMITeR), Universidade Federal de Uberlândia - UFU, Instituto de Química - IQ, Av. João Naves de Ávila, 2121 - Bairro Santa Mônica, Uberlândia, MG, CEP: 38400-902, Brazil.
E-mail addresses: jeffersonferrari@ufu.br, jeffersonferrari@gmail.com (J.L. Ferrari).

https://doi.org/10.1016/j.optmat.2018.07.017
Received 17 April 2018; Received in revised form 5 July 2018; Accepted 8 July 2018
Available online 25 July 2018
0925-3467/

are allowed and intense compared to other transitions, due to spin-orbit coupling effect, the intraconfigurational mixtures, the symmetry of the crystal field and other effects [18]. Depending on the RE^{3+} present, the emissions can occur from the ultraviolet to the infrared region with greater intensity that is dependent on properties of the host matrix [20,21]. These characteristics have attracted attention for use in technological science materials and also to improve the fundamental studies to understand precisely what properties are involved [9]. Among the extensive research on RE^{3+}, there has been a great interest especially in Er^{3+}, due to its *up-conversion* efficiency in the visible region [6]. Furthermore, these ion doped materials also contribute to the transmission signal amplification in the third telecommunications window [22].

Materials doped with Er^{3+} when excited at 980 nm, exhibit an emission band attributed to $^4I_{15/2} \rightarrow {}^4I_{11/2}$, in the infrared region with maximum at 1550 nm, a fundamental characteristic for applications in telecommunications systems and optical amplification devices [23,24]. In this way, the Erbium Doped Fiber Amplifier (EDFA) has gained great attention. The wavelength used in telecommunications systems is positioned in the "Third Window of Telecommunications" (C-Telecom) [25]. This region is divided into three different regions: S band (region between 1460 nm and 1530 nm), C band (region between 1525 nm and 1565 nm) and L band (region between 1570 nm and 1610 nm). Therefore, it is of great industrial interest the development of materials that offer adequate optical and spectroscopic properties to operate in the regions between 1400 nm and 1650 nm [26,27].

In order to contribute to a higher Er^{3+} emission efficiency, since the absorption cross section in the 980 nm region of this ion is very low, around 1.7×10^{-21} cm^2 [11,12], Yb^{3+} is used as sensitizer. The Yb^{3+} absorption band extends over a broader region of wavelength, between 850 and 1080 nm [9,28], being the most intense at 980 nm [8,29]. The co-doping of Yb^{3+} produces enhancement of intense absorption due to the high cross section of Yb^{3+}, about 11.7×10^{-21} cm^2, ten times more efficient than the Er^{3+}, thus increases the optical pumping. Therefore the Yb^{3+} ion can act effectively as a sensitizer of the Er^{3+}, due to resonance conditions between both, together with an efficient energy transfer (ET) from the emission spectral overlap between Yb^{3+} of the transition $^2F_{5/2} \rightarrow {}^2F_{7/2}$ and absorption Er^{3+} of the transition $^4I_{15/2} \rightarrow {}^4I_{11/2}$ [6,12,22]. This process is much more efficient than the excitation directly on Er^{3+}. The efficiency of an optical fiber is related to the increased bandwidth of communication systems (C-Telecom). An optical fiber with a broadened band in this region, allows transporting several wavelengths of light simultaneously. Thus purely optical devices are replacing semiconductor based electronic devices, due to some advantages such as increased transmission speed and distance, broad emission band, resistance to electromagnetic interference, low attenuation of transmitted signal strength and null electrical conductivity. Therefore, fiber based systems are undergoing a period of evolution with the objective of high efficiency in the field of telecommunications, for example, the amplification of the emission signal achieved by the incorporation of rare earth ions in the fiber [4,30].

The selection of the host matrix suitable for the doping of rare earth ions is fundamental in developing efficient materials for optical application, since the matrix and the intentionally added impurity play an important role in the luminescence optical amplification process, pumping efficiency [7,13,31–34], broad band emission, as well as chemical durability, thermal stability [6,35] and mechanical resistance [22].

However, the search for new photoluminescent materials that have these characteristics, led to the investigation of the photoluminescence of RE^{3+} present in aluminum oxide (Al_2O_3), which has been widely studied as a host material to RE^{3+} [36,37]. This material has significant technological importance, because it offers a large window of transparency, from short ultraviolet to the near infrared region [22,38]. It has excellent mechanical properties, good chemical stability [39,40], hardness and refractory properties which makes it an excellent candidate for optical applications [41], amplifiers [42]and lasers [43]. Aluminum oxide is very popular as a dielectric material. It is believed there are more than 15 different crystallographic phases, which can be subjected to a variety of transitions. The most stable structure, *corundum* (α-Al_2O_3), with a gap E_g = 9.4 eV, is the most widely used for practical application and has been thoroughly studied [44–47]. Other phases of alumina, including γ, δ, η, θ, κ β, χ are metastable polymorphs. They are called transition phases, as are the intermediate steps in the process of obtaining the α-phase during calcination [48,49].

Extensive research on the optical properties of Er^{3+} in the aluminum oxide matrix has shown that it is one of the most suitable matrices for Er^{3+} [33,50,51]. The Al_2O_3: Er^{3+}/Yb^{3+} may be prepared by synthetic techniques in which the parameters that affect the optical properties can be varied [52,53]. For example the following techniques may be used ion implantation [28], pulsed laser deposition [54,55], chemical vapor deposition [56], co-precipitation and combustion [3], sol-gel method [32,43,57], among others.

The possible energy emission mechanisms of these materials can be deducted from the energy matching conditions, which are related to the excitation and energy transfer processes of Er^{3+} and Yb^{3+} ions [8]. Among them, the most important mechanism is the phenomenon of *upconversion*. This phenomenon was defined as a nonlinear optical process in which a wave of continuous light of low energy in the near infrared region (NIR) (typically 980 nm) is converted into visible light of higher energy, from the absorption multiple photons or energy transfer [58,59].

In order to obtain materials that have higher photoluminescence efficiency, researchers studied the effect of energy transfer between the Yb^{3+} and Er^{3+} in the host Al_2O_3 matrix. This material was compared to materials doped with Er^{3+}. Thus, they found that co-doping with Yb^{3+} increased the photoluminescence of the material [29]. The excitation mechanism follows the photoluminescence of Er^{3+} in the $^4I_{13/2}$ level with a wavelength of excitation between 890 and 1030 nm. In the sample doped only with Er^{3+}, a narrow band centered at 980 nm can be excited, the absorption band of Er^{3+} and extends from 955 to 1000 nm. In contrast, when the sample is co-doped with Yb^{3+}, the same issue may be activated on a much larger wavelength range with a sharp peak at 975 nm. This peak is characteristic of Yb^{3+}, referring to the level $^2F_{5/2}$ absorption [60]. However, the sample that is co-doped with Yb^{3+} exhibits an effective energy transfer to Er^{3+}, resulting in an absorption band and more intense emission. Thus considering the intensity of photoluminescence in samples co-doped with Yb^{3+}, this materials have potential application in photonic devices.

The understanding of ion emission properties of Er^{3+} and Yb^{3+} as well as their structural and crystalline properties will be conducted in order to evaluate the best photoluminescent properties of the Al_2O_3 doped with these RE^{3+}. The materials will be prepared in two different ways, by a co-precipitation method and by a sol-gel process.

2. Experimental procedure

Initially the synthesis of the Er^{3+}/Yb^{3+} co-doped Al_2O_3 was carried out using a co-precipitation method. In this synthesis, aluminum can rings and alcoholic solutions of erbium chloride, and ytterbium chloride, previously standardized with 0.01 mol L^{-1} EDTA. 0.5 g of aluminum can rings were dissolved in 13 mL of aqueous 5.0 mol L^{-1} HCl with stirring and heating for 15 min at 60 °C. After the rings completely dissolved, the doping was performed with 0.1, 1 and 3 mol% of Er^{3+}, and then co-doping with 1.2 mol% of Yb^{3+}, relative to the total amount of moles of Al^{3+}. Then the ions were precipitated using an ammonium hydroxide solution NH_4OH (Neon – 28–30%). The precipitate was centrifuged and the material was kept in an oven at 100 °C for 4 days. The materials were crushed in an agate mortar to obtain powders which were heat-treated at 400, 600, 900, 1000, 1100 °C for 4 h to obtain the RE^{3+} co-doped aluminum oxide.

Subsequently, the Er^{3+}/Yb^{3+} co-doped Al_2O_3 was synthesized by a sol-gel process using the tri-sec-butoxide aluminum (Aldrich- 97%)

precursor and doped with the same amounts of RE^{3+} reported in the co-precipitation synthesis. Approximately 20 ml of solution (sol) was obtained. Initially the solution was prepared from a mixture of anhydrous ethanol (Êxodo- 99.9%), 2-ethoxyethanol (Sigma- Aldrich- 99%), the precursor aluminum tri-sec-butoxide, two precursor solutions of RE^{3+}, and hydrochloric acid (0.27 mol L^{-1}) as the catalyst solution. This solution was kept with stirring for 15 min. The obtained sol was kept in an oven at 100 °C for two days to obtain the xerogel. The obtained xerogels were crushed in an agate mortar to obtain powders which were heat-treated at 400, 600, 900, 1000, 1100 °C for 4 h to obtain Er^{3+}/Yb^{3+} co-doped Al_2O_3. After obtaining the Er^{3+}/Yb^{3+} co-doped Al_2O_3 materials, prepared by two methods at different temperatures, the materials were characterized. The identification of the crystalline phases of the samples was performed by X-ray diffraction, (XRD). The equipment used was a Shimadzu XRD-6000 diffractometer using Cu Kα radiation (1.5418 Å) at scanning of 0.2°/min from 2θ = 10–80° and graphite monochromator. The particle morphology of the materials were evaluated by SEM using Hitachi TM 3000 benchtop microscope. The emission spectra between 1400 at 1650 nm in the infrared region were carried out using a spectrofluorimeter SPEXF2121/Fluorolog Horiba Jobin Yvon, with an InGaAs detector sensitive from 800 to 1700 nm under excitation at 980 nm using fiber couple laser diode with 2500 mW of power, at room temperature. Subsequently, the upconversion emission spectra in the region between 500 and 700 nm were performed using a photomultiplier tube to monitor the emission in the visible region. A diode laser operating at 980 nm was used as excitation source, varying the power excitation from 2000 at 3500 mW. Based on the energy upconversion emission spectrum, the chromaticity diagram was built.

3. Results and discussion

Based on the XRD analysis, the structural properties and the degree of crystallinity of the material were evaluated fot the two syntheses used in this study. Fig. 1 shows the XRD patterns of the samples of aluminum oxide, synthesized by co-precipitation process doped with 1.2 mol% of Yb^{3+} and (A) 0.1, (B) 1 and (C) 3 mol% of Er^{3+} heat-treated at 400, 600, 900, 1000 and 1100 °C. Results showed that the diffraction pattern of the samples heat-treated at 400 and 600 °C, independent of the concentration of RE^{3+} in the matrix, had broad peaks with the main reflections positioned at 2θ = 45.6° and 66.6°. These peaks are attributed to the γ-Al_2O_3 phase in accordance to the crystallographic cards patterns of JCPSDS N° 00-050-0741. When increasing the heat-treatment temperature the crystallites on the cubic crystalline phase are observed, however there is also the formation of narrow peaks assigned to the crystalline hexagonal phase system assigned to stable corundum alumina (α-Al_2O_3). The phase transition from γ-Al_2O_3 to the hexagonal α-Al_2O_3 phase is provoked by phase transition of the intermediate phases present in the formation of α-Al_2O_3 phase during the heat-treatment process [61]. Therefore, the samples heat-treated at 900, 1000 and 1100 °C, present a mixture of two phases, γ-Al_2O_3 and α- Al_2O_3.

Fig. 2 shows the XRD patterns of the samples of aluminum oxide, synthesized by the sol-gel process. All diffractograms showed peaks that are in accordance to the profile expected for γ-Al_2O_3 phases and α-Al_2O_3, available from ICSD database N° 99836 and 10425, respectively. The results presented in XRD diffractograms show the mixture of two crystalline phases γ-Al_2O_3 and α-Al_2O_3 alumina, at the heat treatment temperature of 900 °C. The same behavior it is observed for the materials obtained by the co-precipitation process.

The thermally treated materials at 1100 °C synthesized by the sol-gel process showed finer peaks relative to the other synthesis. This is due to having a material with a greater degree of crystallinity. In addition, other factors, such as the size of the crystallites composing a sample and the micro-deformation, can also influence the width of the diffraction peaks. Specifically, the diffractogram of the sample based on aluminum oxide doped with 0.1 mol% of Er^{3+} and heat-treated at 1100 °C presents the peaks assigned to the α-Al_2O_3 phase, with the most intense reflections positioned at 2θ = 25.6°, 35.2°, 43.4°, 52.6°, 57.5°, assigned to the hkl planes (102), (104), (113), (204) and (116) respectively. Based on the profiles of XRD patterns for all the samples the crystallinity of the material is observed to increase as a function of heat treatment temperature.

The morphological characteristics of the materials that were heat-treated at different temperatures, synthesized by co-precipitation were analyzed by SEM, (see in in Fig. 3. The micrographs show the different shapes and sizes of the particles. An increase in the heat-treatment temperature causes a formation of larger agglomerates and a heterogeneous morphology is favored, which can may associated with the sintering process during the heat treatment. It is believed that the narrow peaks observed in the XRD of the samples heat-treated at 1100 °C, are associated with the presence of larger particles in the dispersed phase α-Al_2O_3 phase structure. The samples containing different percentages of Er^{3+} and heat-treated at the same temperature exhibit heterogeneous particle morphology.

Fig. 4 shows the micrographs of the materials synthesized by the sol-gel process. An increase in the heat-treatment temperature and Er^{3+} concentration in the host matrix favors the homogeneous morphology and smaller agglomerates, compared to the same materials obtained by the co-precipitation process reported previously.

The materials based on Er^{3+}/Yb^{3+} co-doped Al_2O_3 prepared by the sol-gel process are composed of more homogeneous agglomerates as compared to the same material obtained by the co-precipitation

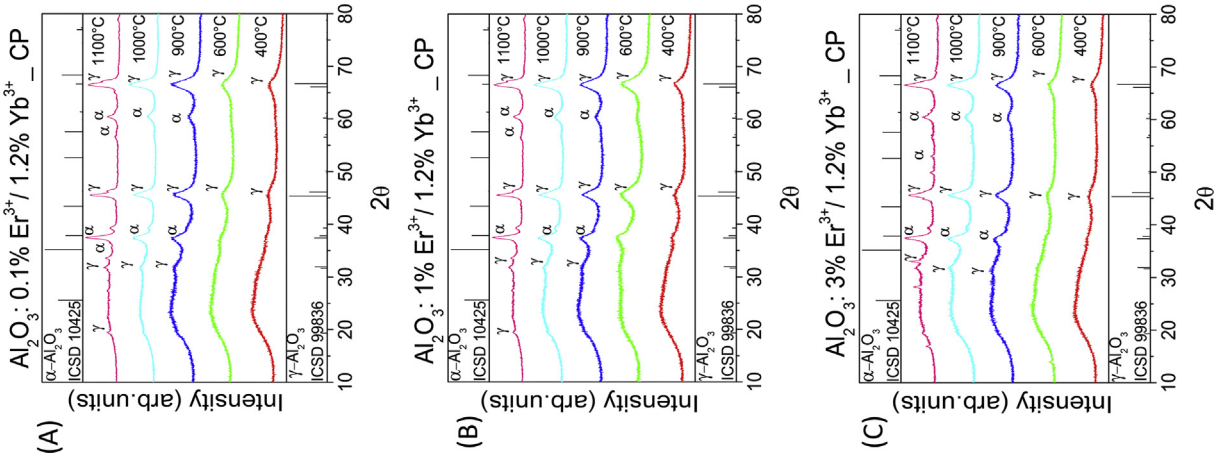

Fig. 1. XRD patterns of the Al_2O_3 synthesized by co-precipitation, heat-treated at 400, 600, 900, 1000 and 1100 °C for 4 h, doped with (A) 0.1, (B) 1 and (C) 3 mol% of Er^{3+} and co-doped with 1.2 mol% of Yb^{3+}.

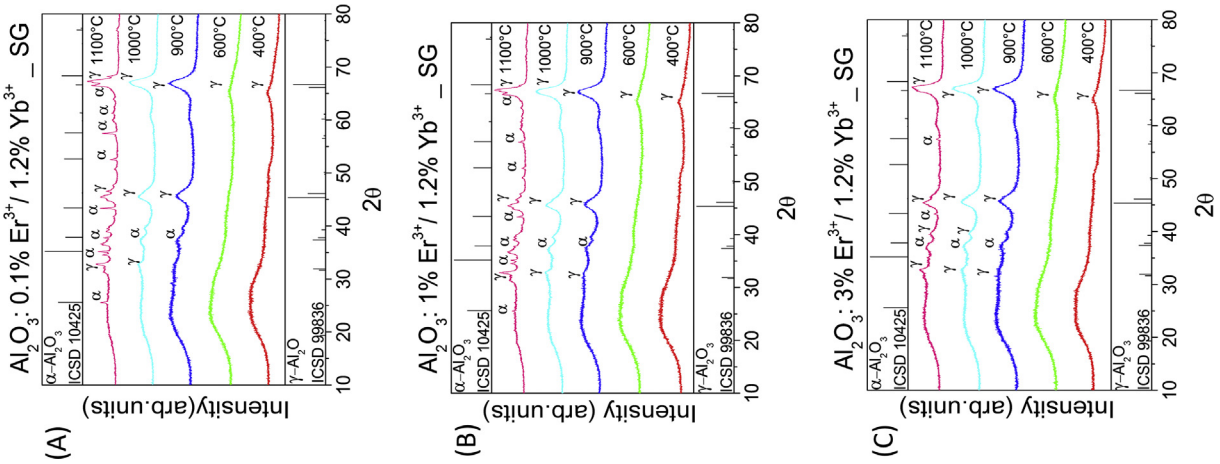

Fig. 2. XRD patterns of the Al_2O_3 synthesized by the sol-gel process, heat-treated at 400, 600, 900, 1000 and 1100 °C for 4 h, doped with (A) 0.1, (B) 1 and (C) 3 mol % of the Er^{3+} and co-doped with 1.2 mol% of the Yb^{3+}.

process. This behavior may be assigned the characteristics that the sol sol-gel process presents. The initial solution, sol, then undergoes a drying process, removing the solvent to obtain the gel formation. This can contribute to more regular seeds during the initial particle formation. With the evaporation of the solvent, the colloidal particles come into contact each other and begin to build a three-dimensional more regular network. In the case of the sol-gel process the solvents used in the synthesis are anhydrous ethanol and ethoxyethanol. These solvents may cause an increased rate of drying, giving agglomerates of smaller particles sizes. These are related to the interconnection of gel structures and tend to be reduced, unlike the synthesis via co-precipitation. In the co-precipitation process larger agglomerates are produced, which may be associated with the amount of hydrogen bonds formed in the aqueous medium as an aqueous solution of HCl was used as the solvent and a catalyst for synthesis.

In order to analyze the photoluminescent properties the materials obtained were analyzed by photoluminescence spectroscopy with an excitation at 980 nm using a diode laser. Initially alumina samples doped with 0.1, 1, or 3 mol% of Er^{3+} and 1.2 mol% of Yb^{3+} were synthesized by a co-precipitation process and heat-treated at different temperatures for 4 h for comparison of the spectroscopy behavior. The analysis of the photoluminescence emission spectra with an excitation at 980 nm, presented the upconversion phenomenon with intense emission in the visible region. In Fig. 5 and Fig. 6 the emission spectra are shown obtained at room temperature of the materials synthesized by co-precipitation, respectively, under the same conditions of excitation, 980 nm.

All bands present in the emission spectra shown in Figs. 5 and 6 for the materials obtained from both synthetics routes, are attributed to intra-configurational f-f transitions of the Er^{3+}. Three emission bands are clearly observed. The two positioned in the green region are assigned to the $^2H_{11/2} \rightarrow {}^4I_{15/2}$ and $^4S_{3/2} \rightarrow {}^4I_{15/2}$ transitions with a maximum emission peak at 525 and a shoulder around 548 nm, respectively. The third one is positioned in the red region of the electromagnetic spectrum, with maximum of emission at 660 nm, attributed the $^4F_{9/2} \rightarrow {}^4I_{15/2}$ transition.

Qualitatively analyzing the emission spectra, the emission band located in the red region is more intense than the emission in the green region, for most spectra except the spectra of the samples containing 1 mol% of Er^{3+} heat-treated at 900 and 1100 °C obtained from the co-

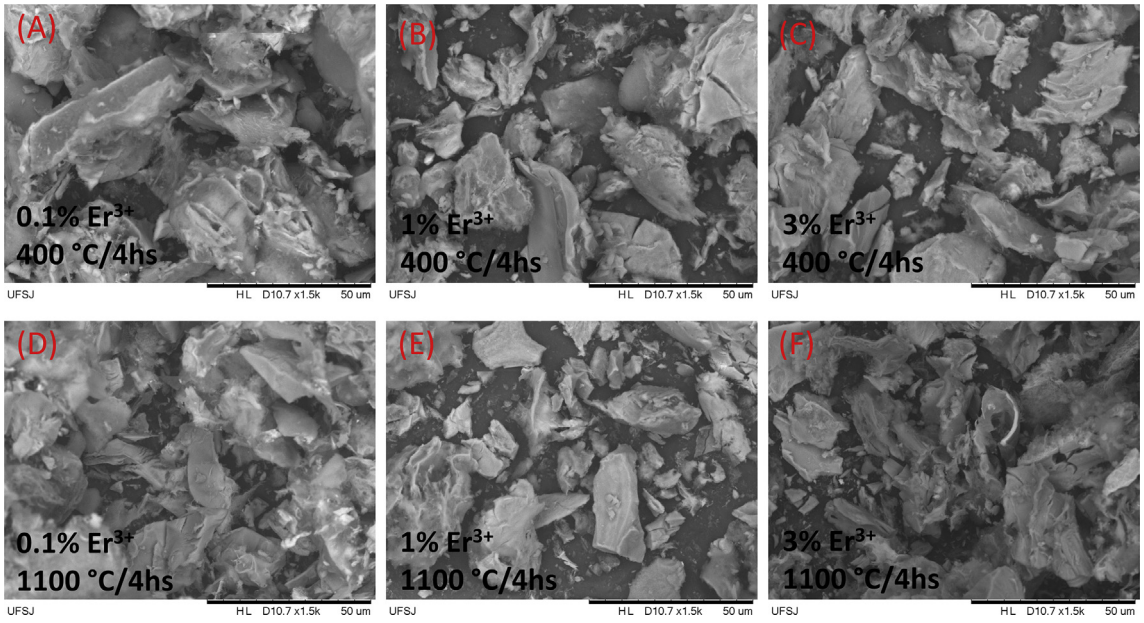

Fig. 3. SEM images of the Al_2O_3, synthesized by co-precipitation, heat-treated at 400 and 1100 °C for 4 h, doped with (A) and (D) 0.1, (B) and (E) 1 and (C) and (F) 3 mol% of the Er^{3+} and co-doped with 1.2 mol% of the Yb^{3+}.

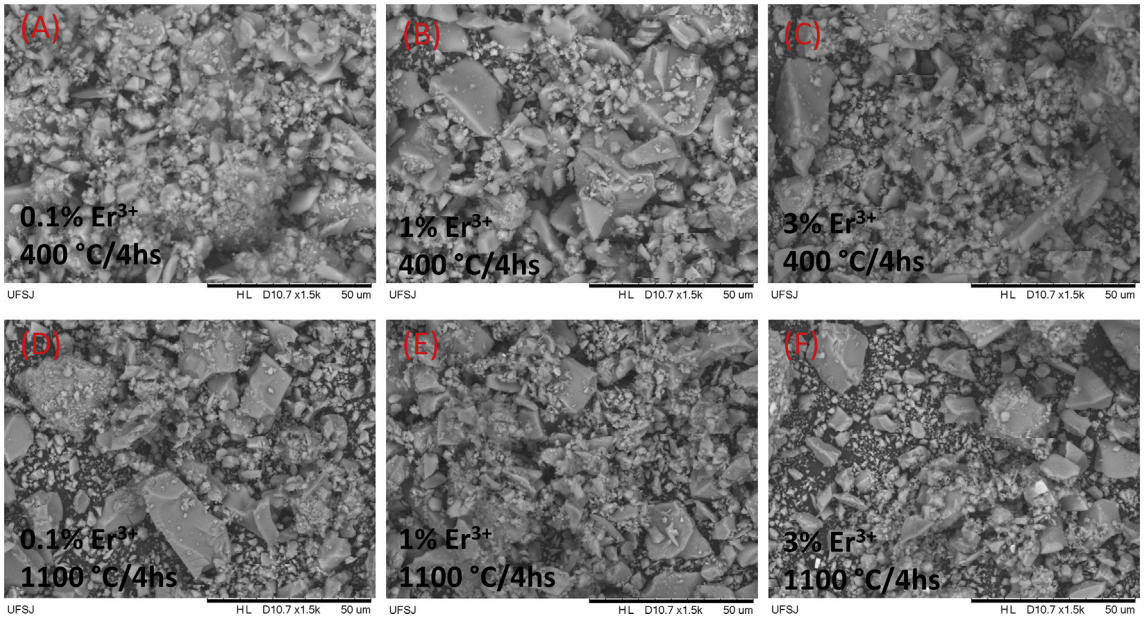

Fig. 4. SEM images of the Al_2O_3, synthesized by the sol-gel process, heat-treated at 400 and 1100 °C for 4 h, doped with (A) and (D) 0.1, (B) and (E) 1 and (C) and (F) 3 mol% of the Er^{3+} and co-doped with 1.2 mol% of the Yb^{3+}.

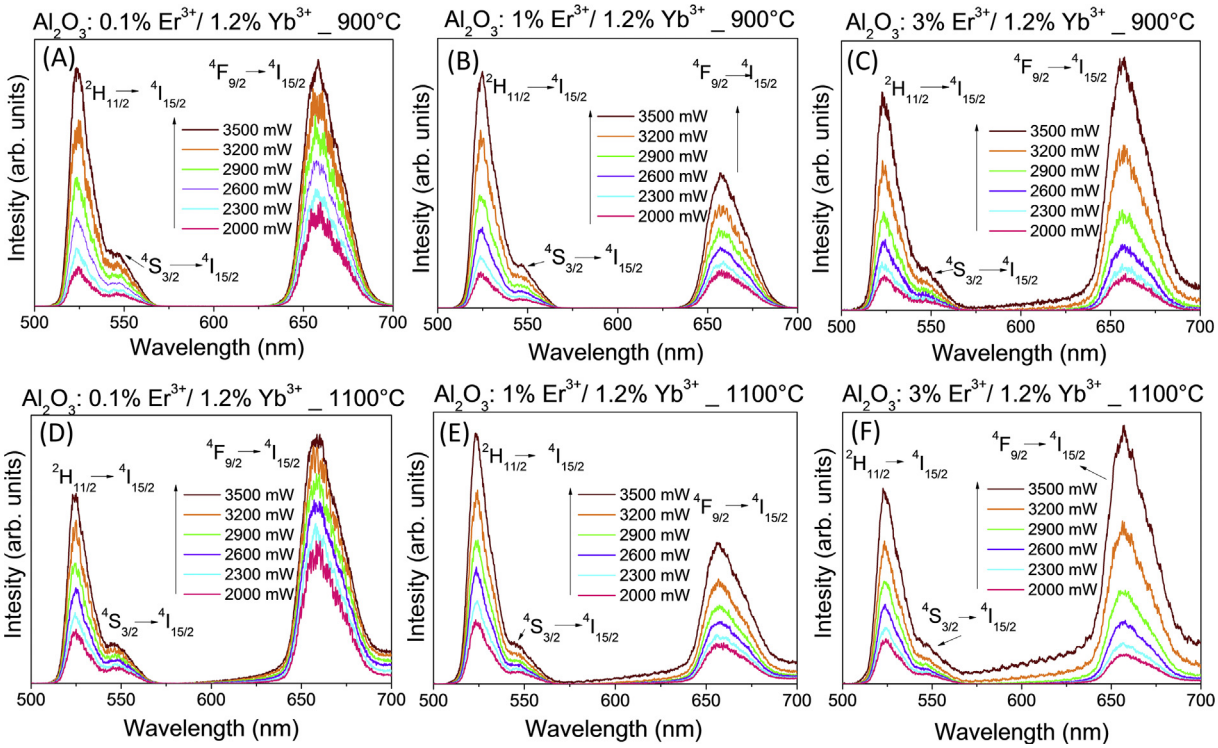

Fig. 5. Photoluminescence emission spectra of Al_2O_3, synthesized by the co-precipitation, heat-treated at 900 and 1100 °C for 4 h, doped with (A) 0.1 and (D) 0.1, (B) and (E) 1 and (C) and (F) 3 mol% of the Er^{3+} and co-doped with 1.2 mol% of the Yb^{3+}.

precipitation method and the samples containing 3 mol% of Er^{3+} heat-treated at 900 °C obtained from the sol-gel process. Nevertheless, this small difference, does not change the main effect present, the width of the emission bands. For all emission bands a similar characteristic is observed in which the band presents inhomogeneous broadening, that can be associated with the position of Er^{3+} in different symmetries in the Al_2O_3 matrix. This associated with the presence of different crystalline phases or different site of symmetry available in the Al_2O_3 host matrix. The broadband emission it is associated to the energy level splitting of Er^{3+} provoked by the different ligand field effect of each symmetry available in the host. Similar effect were observed by Aquino et al. (2013) [4], Ferrari, et al., 2010 [24], Ferrari et al. (2011) [25], Ferrari et al. (2011) [27].

Another very important point aspect is that the intensity of both green and red emission bands increases as a function of excitation laser power. The relative intensity of the green emission to the red emission may be an indication that the energy levels of the red emission are more favorable to populate. The some non radioactive mechanism may be promoting the depopulation of the $^2H_{11/2}$ and $^4S_{3/2}$, (responsible for green emission) to the populating the $^4F_{9/2}$ (responsible for the red

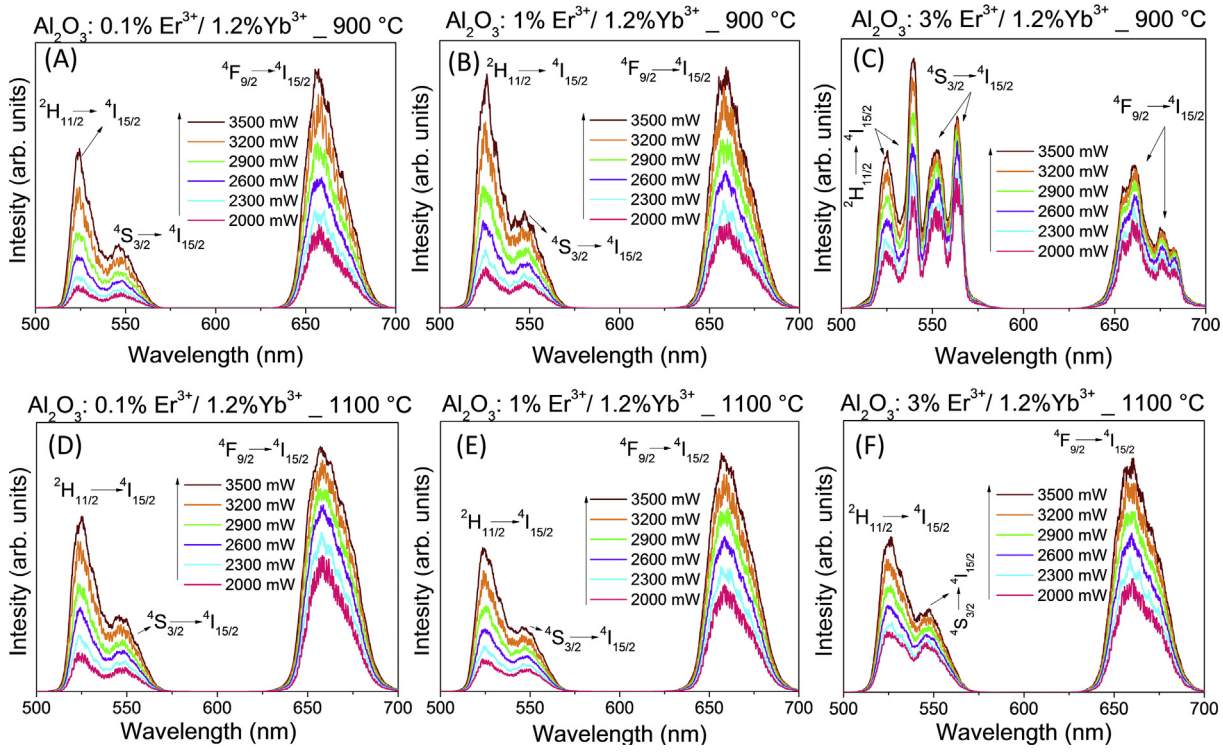

Fig. 6. Photoluminescence emission spectra of Al_2O_3, synthesized by the sol-gel process, heat-treated at 900 and 1100 °C for 4 h, doped with (A) and (D) 0.1, (B) and (E) 1 and (C) and (F) 3 mol% of the Er^{3+} and co-doped with 1.2 mol% of the Yb^{3+}.

emission), or than, the depopulation of the $^4I_{11/2}$ populating the $^4I_{13/2}$, followed by the absorption of a photon at 980 nm populating the $^4F_{9/2}$ and promoting the red emission.

Among many basic mechanisms of upconversion, the two most likely mechanisms for issuing the green and red region under excitation at 980 nm, are identified in the energy level diagram of Er^{3+} and Yb^{3+} in Fig. 7. These mechanisms are Excited State Absorption (ESA) and the Energy Transfer up conversion (ETU) [62–65].

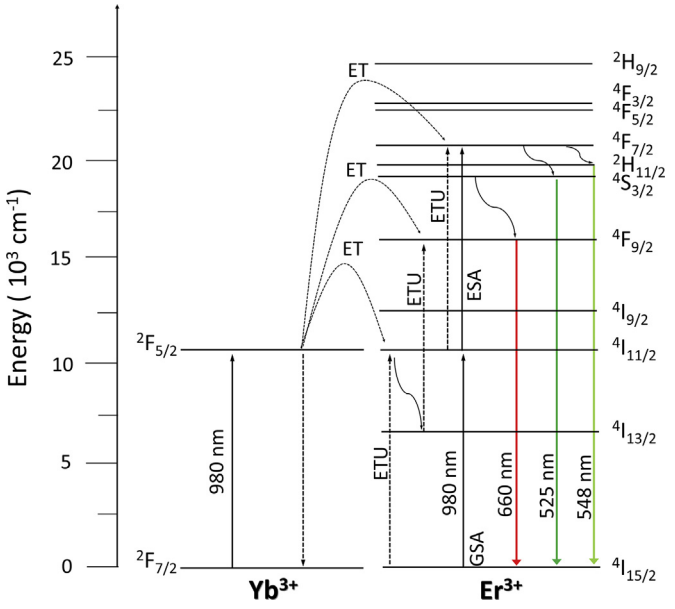

Fig. 7. Energy level diagram of Er^{3+} and Yb^{3+} under excitation at 980 nm, with their emissions in the red and green region. (For interpretation of the references to color in this figure legend, the reader is referred to the Web version of this article.)

The ESA mechanism involves the absorption of one photon, promoting Er^{3+} from the ground state $^4I1_{5/2}$, to the first metastable excited state $^4I_{11/2}$, in a process known as Ground State Absorption (GSA). The long duration of the metastable excited state allows the absorption of a second photon by the same Er^{3+}, which by energy absorption, further promotes the photon excited to the upper excited state, $^4F_{7/2}$. From this excited state, the system may decay non-radiative to the excited levels $^2H_{11/2}$, $^4S_{3/2}$ and $^4F_{9/2}$. Then, Er^{3+} can return to ground state $^4I_{15/2}$, emitting light at 525, 548 and 660 nm, respectively [63,65–68].

On the other hand, the upconversion (UC) process by energy transfer (ETU) involves two close ions. The Yb^{3+} absorbs much more energy than the Er^{3+}, since their absorption cross section is much larger and efficient at 980 nm, as compared to that for Er^{3+}. For this reason the upconversion mainly occurs through the Yb^{3+} energy transfer process, used as a sensitizer for Er^{3+}, with a small contribution by direct absorption of Er^{3+}. Fig. 7 shows the energy levels diagram for Er^{3+} and Yb^{3+} and the mechanisms involved in the UC process. This energy transfer occurs due to an overlap between the absorption band of the transition $^2F_{7/2} \rightarrow {}^2F_{5/2}$ of Yb^{3+} and of the transition $^4I_{15/2} \rightarrow {}^4I_{11/2}$ of Er^{3+}. Then, by decaying, the excited state $^2F_{5/2}$ of Yb^{3+} transfers its energy to $^4I_{11/2}$ level of Er^{3+}. A second photon is promoted to the first metastable excited state $^4I_{11/2}$ up to more energetic states, such as $^4F_{7/2}$. Finally in the same way as it happens for the ESA, those high energy levels can decay for lower levels by non-radiative processes, leading to light emission from the states $^2H_{11/2}$, $^4S_{3/2}$ and $^4F_{9/2}$, in the green region at 525 and 548 nm and in the red region at 660 nm. The highest emission intensity of the band at 660 nm, responsible for issuing the assigned red region the transition $^4F_{9/2} \rightarrow {}^4I_{15/2}$, may be influenced by non-radiative transition $^4I_{11/2} \rightarrow {}^4I_{13/2}$, in addition to the excited level mechanism $^4F_{9/2}$ through non-radiative decays of the $^4S_{3/2}$ level. Another situation that may occur is non-resonant processes, along with surface defects, favoring emission in the red region [69].

To ascertain the emission color of the upconversion emission the chromaticity diagrams were built based on the emission spectra obtained from each sample as a function of the concentration of Er^{3+} in

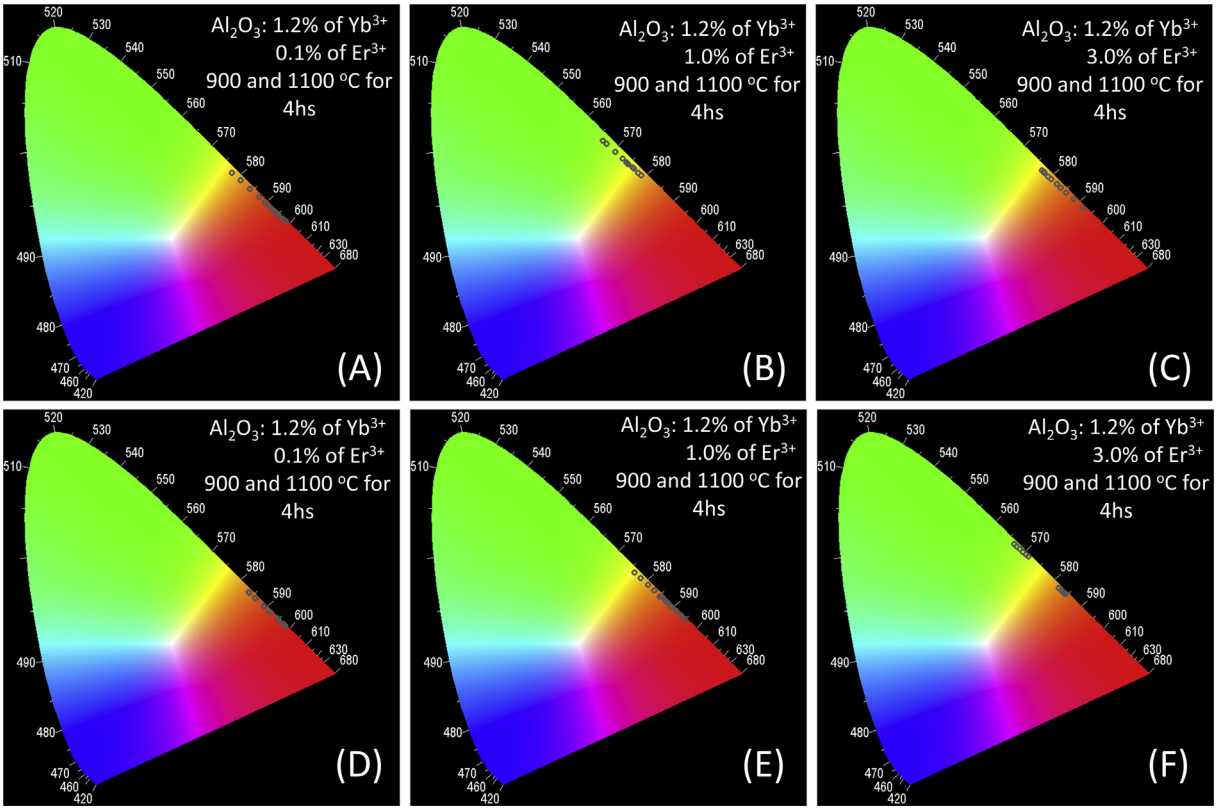

Fig. 8. Chromaticity Diagram of the material synthesized by the co-precipitation _ CP (A), (B) and (C), and materials synthesized by the sol-gel_ SG process (D), (E) and (F). All materials were treated at 600, 900 and 1100 °C, doped with 0.1, 1 and 3 mol% of Er^{3+} and co-doped with 1.2 mol% of Yb^{3+}, with a 980 nm excitation source.

Table 1
Values of X and Y based on the chromaticity diagram, of the materials synthesized by the co-precipitation _ CP.

Power pump (mW)	0.1 mol% Er^{3+}				1 mol% Er^{3+}				3 mol% Er^{3+}			
	900 °C		1100 °C		900 °C		1100 °C		900 °C		1100 °C	
	X	**Y**	**X**	**Y**	**X**	**Y**	**X**	**Y**	**X**	**Y**	**X**	**Y**
2000	0.595	0.393	0.616	0.375	0.498	0.482	0.490	0.488	0.490	0.489	0.485	0.494
2300	0.577	0.410	0.609	0.381	0.477	0.501	0.479	0.479	0.488	0.491	0.489	0.490
2600	0.553	0.431	0.599	0.390	0.454	0.522	0.467	0.509	0.489	0.487	0.499	0.480
2900	0.532	0.451	0.590	0.398	0.436	0.538	0.462	0.513	0.436	0.538	0.519	0.462
3200	0.510	0.471	0.579	0.408	0.415	0.557	0.464	0.511	0.528	0.453	0.558	0.427
3500	0.490	0.489	0.567	0.419	0.407	0.564	0.483	0.494	0.541	0.442	0.579	0.407

Table 2
Values of X and Y based on the chromaticity diagram, of the materials synthesized by the sol-gel_SG process.

Power pump (mW)	0.1 mol% Er^{3+}				1 mol% Er^{3+}				3 mol% Er^{3+}			
	900 °C		1100 °C		900 °C		1100 °C		900 °C		1100 °C	
	X	Y	X	Y	X	Y	X	Y	X	Y	X	Y
2000	0.610	0.380	0.614	0.377	0.557	0.431	0.598	0.393	0.449	0.539	0.529	0.457
2300	0.595	0.394	0.598	0.391	0.543	0.444	0.589	0.401	0.444	0.543	0.536	0.450
2600	0.579	0.409	0.580	0.409	0.527	0.459	0.577	0.411	0.436	0.550	0.535	0.451
2900	0.564	0.423	0.565	0.422	0.512	0.472	0.565	0.422	0.429	0.556	0.532	0.454
3200	0.544	0.441	0.543	0.442	0.494	0.489	0.552	0.434	0.422	0.562	0.526	0.459
3500	0.529	0.455	0.530	0.454	0.480	0.502	0.540	0.445	0.415	0.568	0.519	0.465

the aluminum oxide matrix and heat-treatment temperature. The chromaticity diagrams obtained are depicted in Fig. 8 and the X and Y values obtained are presented in Tables 1 and 2.

Based on upconversion mechanisms proposed in this work and the emission spectra of the materials, it is notable that the band of photoluminescence emission in the red region assigned to $^4F_{9/2} \rightarrow {}^4I_{15/2}$ transition is predominant in most materials reported here. By increasing the ratio of the integrals between the red/green emission bands

Table 3
Relationship between the integral of the area of emission bands $^4F_{9/2} \rightarrow {}^4I_{15/2}/{}^2H_{11/2} \rightarrow {}^4I_{15/2}$ to $^4S_{3/2} \rightarrow {}^4I_{15/2}$, of the materials synthesized by the co-precipitation process, with excitation at 980 nm.

Temperature	%of Er^{3+}	Power Pump (mW)					
		2000	2300	2600	2900	3200	3500
600 °C	0.1	4.89	4.71	4.33	4.17	3.66	3.32
	1	1.97	2.08	1.92	1.88	1.79	1.68
	3	1.69	1.71	1.67	1.70	1.72	1.72
900 °C	0.1	3.06	2.61	2.16	1.84	1.57	1.38
	1	1.42	1.24	1.08	0.97	0.86	0.83
	3	1.30	1.29	1.34	1.49	1.74	1.90
1100 °C	0.1	3.62	3.38	2.96	2.73	2.51	2.24
	1	1.12	1.06	1.00	0.98	1.02	1.08
	3	1.13	1.20	1.34	1.53	2.01	2.28

Table 4
Relationship between the integral of area of the emission bands $^4F_{9/2} \rightarrow {}^4I_{15/2}/{}^2H_{11/2} \rightarrow {}^4I_{15/2}$ to $^4S_{3/2} \rightarrow {}^4I_{15/2}$, of the materials synthesized by the sol-gel process, with excitation at 980 nm.

Temperature	% of Er^{3+}	Power Pump (mW)					
		2000	2300	2600	2900	3200	3500
600 °C	0.1	1.10	1.08	1.03	0.98	0.93	0.76
	1	1.47	1.42	1.38	1.29	1.30	1.39
	3	0.42	0.38	0.35	0.34	0.33	0.34
900 °C	0.1	3.31	2.89	2.52	2.23	1.93	1.72
	1	1.99	1.80	1.60	1.45	1.29	1.17
	3	0.60	0.59	0.57	0.55	0.53	0.52
1100 °C	0.1	3.54	3.04	2.56	2.27	1.90	1.72
	1	2.93	2.71	2.46	2.24	2.02	1.85
	3	1.59	1.70	1.70	1.68	1.62	1.56

assigned to the transition $^4F_{9/2} \rightarrow {}^4I_{15/2}$ (responsible for the red region) and the transitions $^2H_{11/2} \rightarrow {}^4I_{15/2}$ to $^4S_{3/2} \rightarrow {}^4I_{15/2}$ (responsible for the green region), respectively, it is possible to analyze the behavior of the intensity of the emission for each of the bands. The ratios between the bands as a function of power pump for materials synthesized by co-precipitation method and the sol-gel process are presented in Tables 3 and 4, respectively.

The emission spectra in the infrared region between 1400 nm and 1650, of the heat-treated materials at 400, 600, 900 and 1100 °C for 4 h, synthesized by the co-precipitation and sol-gel process were collected under excitation at 980 nm. All samples doped with 0.1; 1 and 3 mol% Er^{3+}, and co-doped with 1.2 mol% of Yb^{3+}, showed the maximum of emission at 1530 nm, assigned to transition from the $^4I_{13/2} \rightarrow {}^4I_{15/2}$ of Er^{3+} known as the C-telecom band.

Fig. 9 shows the emission spectrum of the infrared region of the Al_2O_3 based materials: x mol% Er^{3+}/1.2 mol% Yb^{3+} where (x = 0.1, 1 and 3%), heat treated 1100 °C, synthesized by the sol-gel process. Different spectral profiles and half-height bandwidth values (FWHM) can be observed, as a result of the influence of Er^{3+} concentration on the matrix. With an increase in the Er^{3+} concentration the processes of non-radiative energy transfer can occur between the Er^{3+} to another nearest neighbor ion through the cross relaxation. The increasing the concentration of TR^{3+} favors the decrease of the distance between them and consequently, increases the process of cross relaxing. These mechanisms are presented by Lupei in 1991 [70].

In Table 5 the FWHM values of the emission bands around 1530 nm of all the materials reported in this work are presented. Unlike materials synthesized by the sol-gel process, which exhibit heat treated material at 1100 °C with the highest FWHM value, without co-precipitation

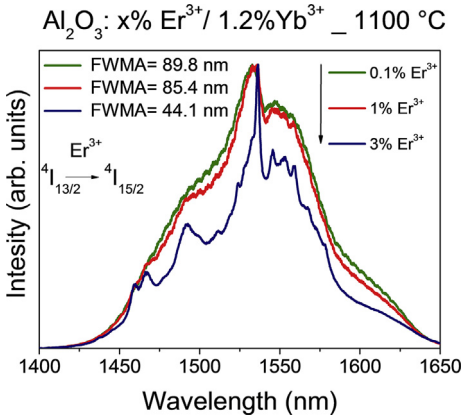

Fig. 9. Infrared emission spectra in the region between 1400 and 1650 nm of Al_2O_3 doped with 0.1, 1 and 3 mol% of Er^{3+} and co-doped with 1.2 mol% of Yb^{3+}, synthesized by the sol-gel process, heat-treated at 1100 °C for 4 h under excitation at 980 nm at room temperature.

Table 5
Values of FWHM of the emission band attributed to the transition $^4I_{13/2} \rightarrow {}^4I_{15/2}$ Er^{3+}, with maximum positioned around 1532 nm know as Telecom-C region.

Temperature	mol% of Er^{3+}	Co-Precipitation method FWHM (nm)	Sol-Gel Process FWHM (nm)
400 °C	0.1	68.37	63.75
	1	**80.17**	65.59
	3	**73.21**	70.45
600 °C	0.1	44.07	63.41
	1	48.01	50.36
	3	50.19	50.15
900 °C	0.1	55.16	53.20
	1	57.09	56.84
	3	66.20	58.83
1100 °C	0.1	54.74	**89.76**
	1	67.30	**85.37**
	3	65.11	44.06

process, the highest value was found in the thermally treated material at 400 °C. In view of this, it can be concluded that the width at half height is influenced by the temperature at which the materials are treated. The presence of the γ-Al_2O_3 phase in the thermally treated material at 400 °C obtained by the co-precipitation process, presents a structure with a tetrahedral distortion. It is considered in the literature that the γ-Al_2O_3 phase is a structure of a spinel ($MgAl_2O_4$) with defects. These defects occur because the stoichiometry of Al and O do not fit into the spinel structure, resulting in distorted sites that can accommodate the RE^{3+} [71,72]. These different symmetries containing the RE^{3+} cause an inhomogeneous broadening in the band emission resulting in the formation of a broadband. The materials obtained by the sol-gel process at 1100 °C present a mixture of phases γ and α-Al_2O_3. Therefore, the mixture between the two phases, γ and α, cause the existence of multiple symmetry sites. Thus, when the ions occupy these structures, the ions are located at different locations of symmetry, resulting in an inhomogeneous enlargement, promoting the formation of a wide emission range in the region of 1530 nm. Materials that have a broadband emission in the 1530 nm region, presented by Er^{3+}, are promising for application as optical amplifiers for C-band telecommunications because they increase the area of information transmission channels [30].

4. Conclusion

The results show that it was possible to monitor the achievement of Al_2O_3 doped with different concentrations of Er^{3+}, via two simple, quick and cost-effective syntheses. In addition to these advantages, the synthesis process carried out by the co-precipitation method was also a recycling method for rings aluminum cans, and low power consumption for the preparation of materials with important technological applications. The materials presented efficiency in energy absorption in the infrared, with light emission in the visible region. The upconversion emission spectra showed broad bands, indicating that the Er^{3+}, is located in different sites of symmetry, because of the mixture of the α and γ phases obtained in XRD. All emissions observed in both syntheses, presented the bands assigned the $^2H_{11/2} \rightarrow {}^4I_{15/2}$ and $^4S_{3/2} \rightarrow {}^4I_{15/2}$ transitions with a maximum emission intensity at 525 and 548 nm respectively. These two transitions are responsible for issuing the emission in the green region of the electromagnetic spectrum region. A third band was also observed with a peak emission at 660 nm, attributed the $^4F_{9/2} \rightarrow {}^4I_{15/2}$ transition responsible for emission in the red region. Considering the analysis of the emission spectra, one can see that the emission band located in the red region is more intense than the emission in the green region, in the materials which contains a lower concentration of Er^{3+}. Moreover, they showed an intense emission in the infrared region around 1530 nm, with a value of 89.8 nm demonstrating an excellent candidate in developing optical amplifiers in the Telecommunications 3rd window (C- band). Therefore, these synthesized materials have potential application in photonic devices, because of their photoluminescent properties.

Acknowledgments

This work was supported by the FAPEMIG, CAPES, CNPq and FINEP. This work is a collaboration research project of members of the Rede Mineira de Química (RQ-MG) supported by FAPEMIG (Project: CEX - RED-00010-14). The authors also thanks to Dr. Daniel F. Segura (danielfsegura@outlook.com) for his work on the digital art of graphical abstract.

References

[1] T.A. Kim, L.Q. Minh, N. V, T. T Huong, N. T Huong, C. Barthou, W. Strek, Nanomaterials containing rare-earth ions Tb, Eu, Er and Yb: preparation, optical properties and application potential, J. Lumin. 102–103 (2003) 391–394.
[2] Q.Y. Zhang, X.Y. Huang, Recent progress in quantum cutting phosphors, Prog. Mater Sci. 55 (2010) 353–427.
[3] A. Patra, Study of photoluminescence properties of Er^{3+} ions in SiO_2–GeO_2 and Al_2O_3 nanoparticles, Solid State Commun 132 (2004) 299–303.
[4] F.T. Aquino, J.L. Ferrari, S.J.L. Ribeiro, A. Ferrier, P. Goldner, R.R. Gonçalves, Broadband NIR emission in novel sol–gel Er^{3+}-doped SiO_2–Nb_2O_5 glass ceramic planar waveguides for photonic applications, Opt. Mater 35 (2013) 387–396.
[5] W.M. Azevedo, D.D. Carvalho, E.A. Vasconcelos, E.F. Silva Jr., Photoluminescence characteristics of rare earth-doped nanoporous aluminum oxide, Appl. Surf. Sci. 234 (2004) 457–461.
[6] J.K. Krebs, U. Happek, Yb^{3+} energy levels in á-Al_2O_3, J. Lumin 94–95 (2001) 65–68.
[7] B. Dong, T. Yang, M.K. Lei, Optical high temperature sensor based on green up-conversion emissions in Er^{3+} doped Al_2O_3, Sens. Actuators B Chem. 123 (2007) 667–670.
[8] S.W. Yung, H.J. Lin, Y.Y. Lin, R.K. Brow, Y.S. Lai, J.S. Hornga, T. Zhang, Concentration effect of Yb^{3+} on the thermal and optical properties of Er^{3+}/Yb^{3+}-codoped ZnF_2–Al_2O_3–P_2O_5glasses, Mater. Chem. Phys. 117 (2009) 29–34.
[9] A.J. Kenyon, Recent developments in rare-earthdoped materials for optoelectronics, Prog. Quantum Electron 26 (2002) 225–284.
[10] T. Aitasalo, P. Deren, J. Holsa, H. Jungner, J.-C. Krupa, M. Lastusaari, J. Legendziewicz, J. Niittykoski, W. Strek, Persistent luminescence phenomena in materials doped with rare earth ions, J. Solid State Chem. 171 (2003) 114–122.
[11] S. Hraiech1, M. Ferid1, Y. Guyot, G. Boulon, Structural and optical studies of Yb^{3+}, Er^{3+} and Er^{3+}/Yb^{3+} co-doped phosphate glasses, J. Rare Earths 31 (2013) 685.
[12] M.Y. Yoo, J.H. Lee, H.M. Jeong, K.S. Lim, P. Babu, Enhancement of photo-luminescence and upconversion in Er–Yb codoped nanocrystalline glass–ceramics, Opt. Mater 35 (2013) 1922–1926.
[13] B. Dong, X.J. Wang, C.R. Li, Z.Q. Feng, J.Z. Zheng, Arc discharge synthesis and up-conversion emissions of Er^{3+} doped Al_2O_3 nanoparticles, Mater. Lett. 62 (2008) 3171–3173.
[14] Z. Zang, All-optical switching in Sagnac loop mirror containing an ytterbium-doped fiber and fiber Bragg grating, Appl. Opt 52 (2013) 5701–5706.
[15] Z.-G. Zang, Y.-J. Zhang, Low-switching power (< 45 mW) optical bistability based on optical nonlinearity of ytterbium-doped fiber with a fiber Bragg grating pair, J. Mod. Opt. 59 (2012) 161–165.
[16] J.K. Krebs, S.P. Feofilov, A.A. Kaplyanskii, R.I. Zakharchenya, U. Happek, Non-radiative relaxation of Yb^{3+} in highly porous γ-Al_2O_3, J. Lumin 83–84 (1999) 209–213.
[17] J.D. Lee, Química inorgânica: um novo texto conciso, Edgard Blucher, São Paulo, 1980.
[18] D.F. Shriver, P.W. Atkins, Química Inorgânica, terceira ed., Bookman, Porto Alegre, 2003.
[19] H. Lian, Z. Hou, M. Shang, D. Geng, Y. Zhang, J. Lin, Rare earth ions doped phosphors for improving efficiencies of solar cells, Energy 57 (2013) 270–283.
[20] H.C. Jung, J.Y.G. Park, R. Seeta, R. Raju, H. Jung, B.K. Moon, J.H. Kim, H.Y. Choi, Crystalline structure dependence of luminescent properties of Eu^{3+}-activated Y_2O_3–Al_2O_3 system phosphors, Curr. Applied Phys. 9 (2009) S217–S221.
[21] I.L.V. Rosa, A.P. Maciel, E. Longo, E.R. Leite, J.A. Varela, Synthesis and photo-luminescence study of $La_{1.8}Eu0.2O_3$ coating on nanometric α-Al2O3, Mat. Res. Bull. 41 (2006) 1791–1797.
[22] B. Dong, C.R. Li, M.K. Lei, Green and red up-conversion emissions of Er^{3+}–Yb^{3+}-codoped Al_2O_3 powders prepared by the nonaqueous sol–gel method, J. Lumin 126 (2007) 441–446.
[23] D. Manzani, M. Montesso, C.F. Mathias, K.V. Krishanaiah, S.J.L. Ribeiro, M. Nalin, Visible up-conversion and near-infrared luminescence of Er^{3+}/Yb^{3+} co-doped $SbPO_4$-GeO_2 glasses, Opt. Mater 57 (2016) 71–78.
[24] J.L. Ferrari, K.O. Lima, L.J.Q. Maia, R.R. Gonçalves, Sol-gel preparation of near-infrared broadband emitting Er^{3+}-doped SiO_2-Ta_2O_5 nanocomposite films, Thin Solid Films 519 (2010) 1319–1324.
[25] J.L. Ferrari, K.O. Lima, L.J.Q. Maia, S.J.L. Ribeiro, R.R. Gonçalves, Structural and spectroscopic properties of luminescent Er3+-Doped SiO_2-Ta_2O_5, J. Am. Ceram. Soc. 94 (2011) 1230–1237.
[26] P.C. Becker, N.A. Olsson, J.R. Simpson, Erbium-doped Fiber Amplifiers: Fundamentals and Technology, primeira ed, Academic Press Digital, 1999.
[27] J.L. Ferrari, K.O. Lima, L.J.Q. Maia, S.J.L. Ribeiro, A.S.L. Gomes, R.R. Gonçalves, Broadband NIR emission in sol–gel Er^{3+}-Activated SiO_2–Ta_2O_5 glass ceramic planar and channel waveguides for optical application, J. Nanosci. Nanotechnol. 11 (2011) 2540–2544.
[28] X.J. Wang, M.K. Lei, T. Yang, B.S. Cao, Coherent effect of Er^{3+}–Yb^{3+} co-doping on enhanced photoluminescence properties of Al_2O_3 powders by the sol–gel method, Opt. Mater 26 (2004) 253–259.
[29] C. Strohhofer, A. Polman, Absorption and emission spectroscopy in Er^{3+}–Yb^{3+} doped aluminum oxide waveguides, Opt. Mater 21 (2003) 705–712.
[30] Y. Chu, J. Ren, J. Zhang, G. Peng, J. Yang, P. Wang, L. Yuan, Ce^{3+}/Yb^{3+}/Er^{3+} triply doped bismuth borosilicate glass: a potential fiber material for broadband near-infrared fiber amplifiers, Nature Photonics 6 (2016) 33865.
[31] F. Auzel, D. Pecile, Absolute efficiency for IR to blue conversion materials and theoretical prediction for optimized matrices, J. Lumin. 11 (1976) 321–330.
[32] T. Yang, H. Wang, M.K. Lei, Phase transition of Er^{3+}-doped Al_2O_3 powders prepared by the non-aqueous sol–gel method, Mater. Chem. Phys. 95 (2006) 211–217.
[33] X.J. Wang, M.K. Lei, T. Yang, H. Wang, Phase structure and photoluminescence properties of Er^{3+}-doped Al_2O_3 powders prepared by the sol–gel method, Opt. Mater 26 (2004) 247–252.
[34] Z. Zhu, D. Liu, H. Liu, G. Li, J. Du, Z. He, Fabrication and luminescence properties of Al_2O_3:Tb^{3+} microspheres via a microwave solvothermal route, J. Lumin 132 (2012) 261–265.
[35] N. Rakov, G.S. Maciel, W.B. Lozano, C.B. Araújo, Europium luminescence enhancement in Al_2O_3:Eu^{3+} powders prepared by direct combustion synthesis, J. Appl. Phys. 101 (2007) 036102.
[36] E.F. Huerta, I. Padilla, R. Martinez, J.L. Hernandez, U. Caldino, C. Falcony, Extended decay times for the photoluminescence of Eu^{3+} ions in aluminum oxide films through interaction with localized states, Opt. Mater 34 (2012) 1137–1142.
[37] N. Rakov, G.S. Maciel, Photoluminescence analysis of α-Al_2O_3 powders doped with Eu^{3+} and Eu^{2+} ions, J. Lumin 127 (2007) 703–706.
[38] T. Ishizaka, R. Nozaki, Y. Kurokawa, Luminescence properties of Tb^{3+} and Eu^{3+}-doped alumina films prepared by sol-gel method under various conditions and sensitized luminescence, J. Phys. Chem. Solids 63 (2002) 613–617.
[39] L. Trinkler, B. Berzina, D. Jakimovica, J. Grabis, I. Steins, UV-light induced luminescence processes in Al_2O_3 bulk and nanosize powders, Opt. Mater 32 (2010) 789–795.
[40] N. Rakov, G.S. Maciel, Enhancement of luminescence efficiency of f–f transitions from Tb^{3+} due to energy transfer from Ce^{3+} in Al_2O_3 crystalline ceramic powders prepared by low temperature direct combustion synthesis, Chem. Phys. Lett. 400 (2004) 553–557.
[41] W.L. Feng, Theoretical investigation on the optical absorption spectra and local lattice structure of α-Al_2O_3:Yb^{3+} crystals, Optik Int. J. Light Electron Optics 120 (2009) 696–698.
[42] P.A. Tanner, K.L. Wong, Y. Liang, Multiple phase production on doping Er^{3+} into α-Al_2O_3, Chem. Phys. Lett. 399 (2004) 15–19.
[43] M. Mahnke, S. Wiechmann, H.J. Heider, O. Blume, J. Müller, Aluminum oxide doped with erbium, titanium and chromium for active integrated optical applications, Int. J. Electronics Commun. 55 (2001) 342–348.
[44] L. Trinkler, B. Berzina, D. Jakimovica, J. Grabis, I. Steins, Peculiarities of photo-luminescence of Al_2O_3 bulk and nanosize powders at low temperatures, Opt. Mater 33 (2011) 817–822.

[45] L. Trinkler, B. Berzina, Z. Jevsjutina, J. Grabis, I. Steins, C.J. Baily, Photoluminescence of Al_2O_3 nanopowders of different phases, Opt. Mater 34 (2012) 1553–1557.
[46] P.G. Li, M. Lei, W.H. Tang, Raman and photoluminescence properties of α-Al_2O_3microcones with hierarchical and repetitive superstructure, Mater. Lett. 64 (2010) 161–163.
[47] S. Cava, S.M. Tebcherani, S.A. Pianaro, C.A. Paskocimas, E. Longoc, J.A. Varela, Structural and spectroscopic analysis of α-Al_2O_3 to -Al_2O_3-$CoAl_2O_4$ phase transition, Mater. Chem. Phys. 97 (2006) 102–108.
[48] E. Gubelin, Internacional World of Gemstones, ABC-Verlag, 1974.
[49] D.H.S. Reis, J.M.M. Buarque, M.A. Schiavon, E. Pecoraro, S.J.L. Ribeiro, J.L. Ferrari, Simple and cost-effective method to obtain RE^{3+} doped Al_2O_3 for possible photonic applications, Ceram. Int. l41 (2015) 10406–10414.
[50] X. Multone, Y. Luo, P. Hoffmann, Er-doped Al_2O_3 thin films deposited by high-vacuum chemical vapor deposition (HV-CVD), Mater. Sci. Eng. B 146 (2008) 35–40.
[51] J.K.R. Weber, J.J. Felten, B. Cho, P.C. Nordine, Glass fibres of pure and erbium- or neodymium-doped yttria–alumina compositions, Letter. Nature 393 (1998) 769–771.
[52] H. Wang, M.K. Lei, Enhanced optical activation of Er^{3+} in Er^{3+}-doped Al_2O_3 powders by Y^{3+} codoping in a sol–gel method, J. Lumin. 129 (2009) 110–113.
[53] E. Cattaruzza, M. Back, G. Battaglin, P. Riello, E. Trave, Er-doped alumina crystalline films deposited by radiofrequency magnetron co-sputtering, Opt. Mater 33 (2011) 1135–1138.
[54] M.J. Castro, A.S. Garci, R. Serna, C.N. Afonso, J.G. Lopez, Optical activation of Er^{3+} in Al_2O_3 during pulsed laser deposition, Opt. Mater 29 (2007) 539–542.
[55] M.Y. Tsvetkov, S.M. Kleshcheva, M.I. Samoilovich, N.V. Gaponenko, A.N. Shushunov, Erbium photoluminescence in opal matrix and porous anodic alumina nanocomposites, Microelectron. Eng 81 (2005) 273–280.
[56] A.J. Kenyom, C.E. Chryssou, T.M. Smeeton, C.J. Humphreys, D.E. Hole, Sensitisation of erbium luminescence in erbium-implanted alumina, Opt. Mater 28 (2006) 655–659.
[57] U. Happek, S.A. Basunb, J. Choi, J.K. Krebs, M. Raukas, Electron transfer processes in rare earth doped insulators, J. Alloys Compd 303–304 (2000) 198–206.
[58] X. Wang, H. Chang, J. Xie, B. Zhao, B. Liu, S. Xu, W. Pei, N. Ren, L. Huang, W. Huang, Recent developments in lanthanide-based luminescent probes, Coord. Chem. Rev. 273 (2014) 201–212.
[59] S. Hong, S. Kegang, Z. Enwei, B. Yanjie, C. Yan, X. Xiaoling, W. Shenguo, F. Jing, W. Shicheng, Surface bioactivity modification of titanium by CO_2 plasma treatment and induction of hydroxyapatite: in vitro and in vivo studies, Appl. Surf. Sci. 257 (2011) 1813–1823.
[60] J.K. Krebs, U. Happek, Yb^{3+} energy levels in α-Al_2O_3, J. Lumin. 94–95 (2011) 65–68.
[61] A. Vázquez, T. López, R. Gómez, Bokhimi, A. Morales, O. Novaro, X-ray diffraction, FTIR, and NMR characterization of sol–gel alumina doped with lanthanum and cerium, J. Solid State Chem. 128 (1997) 161.
[62] S. Xu, S. Huang, Q. He, L. Wang, Upconversion nanophosphores for bioimaging, Trends. Anal. Chem. 66 (2015) 72–79.
[63] H. Chen, W. Yong, Y. Fei, X. Juan, Y. Zhang, L. Wang, Inner filter effect of gold nanoparticles on the fluorescence of rare-earth phosphate nanocrystals and its application for determination of biological aminothiols, J. Lumin 141 (2013) 33–37.
[64] M. Wang, G. Abbineni, A. Clevenger, C. Mao, S. Xu, Upconversion nanoparticles: synthesis, surface modification and biological applications, Nanomedicine 7 (2011) 710–729.
[65] F. Auzel, Upconversion and Anti-Stokes processes with f and d ions in solids, Chem. Rev. 104 (2004) 139–173.
[66] M. Haase, H. Schaefer, Upconverting nanoparticles, Angew. Chem. Int. Ed. 50 (2011) 5808–5829.
[67] L.A. Riseberg, H.W. Moos, Multiphonon orbit-lattice relaxation of excited states of rare-earth ions in crystals, Phys. Rev. 174 (1968) 429–438.
[68] F. Wang, D. Banerjee, Y. Liu, X. Chen, X. Liu, Upconversion nanoparticles in biological labeling, imaging, and therapy, Analyst 135 (2010) 1839–1854.
[69] R. Balda, J. Fernández, M.A. Arriandiaga, J.M. Fdez-Navarro, Infrared to visible upconversion of Er^{3+} and Er^{3+}/Yb^{3+}codoped lead–niobium–germanate glasses, Opt. Mater 25 (2004) 157–163.
[70] V. Lupei, Laser processes and energy transfers, J. Lumin. 48 (1991) 157–165.
[71] Y. Onishi, T. Nakamura, S. Adachi, Tb^{3+} ion doping into Al_2O_3: solubility limit and iluminescence properties, J. Appl. Phys. 55 (2016) 112401.
[72] S. Blonski, S.H. Garofalini, Molecular dynamics simulations of α-alumina and γ-alumina surfaces, Surface Sci. 295 (1993) 263–274.